Enhancing Participation of Widespread Distributed Energy Storage Systems in Frequency Regulation through Partitioning-based Control

Yujun Lin, Haowen Luo, Yin Chen, Qiufan Yang, Jianyu Zhou, and Xia Chen, *Senior Member*, *IEEE*

***Abstract*—In recent years, a significant number of distributed small-capacity energy storage (ES) systems have been integrated into power grids to support grid frequency regulation. However, the challenges associated with high-dimensional control and synergistic operation alongside conventional generators remain unsolved. In this paper, a partitioning-based control approach is developed for the participation of widespread distributed ES systems on frequency control in power systems. The approach comprises a network partitioning method and a two-layer frequency control scheme. The partitioning method utilizes a community detection algorithm in which the weights between the buses are calculated based on the electrical distances. After partitioning the buses into different groups, an optimization-based frequency control system with two layers is established to aggregate and dis-aggregate the inertia and droop coefficients so that frequency regulation and economical operation can be achieved. The effectiveness of the proposed method is demonstrated through numerical simulations on an IEEE 39-bus system. The results confirm the successful elimination of frequency deviations and low operating cost of the proposed approach.**

***Index Terms*—Community detection algorithm, distributed control, energy storage, frequency response.**

I. Introduction

To achieve carbon neutrality, renewable energy sources such as wind and solar power systems are being extensively promoted in China [1]. However, the increasing integration of renewable energy into power grids can lead to undesired power fluctuations, which may threaten the frequency security of power systems [2]–[5]. To address this problem, distributed small-capacity energy storage (ES) systems have been introduced to reduce transmission losses and investment and operating costs, and to increase installation location flexibility [6]. However, the widespread installation of small-capacity distributed ES systems presents two significant technical challenges for frequency control: 1) line impedance variations can result in different frequency response characteristics among buses, which increases control complexity [7]; and 2) controlling a large number of ES systems results in a high-dimensional optimization problem, which poses a significant computational burden [8]. It is therefore necessary to address the frequency control challenges that arise from the widespread deployment of small-capacity distributed ES systems.

There is an abundant pool of literature on frequency control methods for widely distributed ES systems. In [9]–[11], automatic generation control (AGC) signals for secondary frequency regulation are generated using PI controllers. In particular, reference [9] designs a finite-time consensus algorithm to allocate AGC signals to individual ES systems using sparse communication networks, whereas in [10], a battery management system is developed to address the ES sizing issue. In [11], a progressive state recovery strategy is proposed to optimize frequency control in electric vehicles (EVs) by considering charging preferences. It should be noted that the above methods are based on a simplified single-machine frequency response model. In [12], the inertia coefficients of distributed energy resources are optimally tuned in real time using distributed controllers to improve the frequency response metrics. In [13]–[19], the optimization problems of the converter inertia and droop are solved to guarantee frequency security and system stability. However, centralized optimization methods usually suffer from long computation time, considerable communication overload, privacy issues, and low scalability. In contrast, distributed methods,

Received: January 30, 2024
Accepted: August 25, 2024
Published Online: January 1, 2025
Yujun Lin, Qiufan Yang, Jianyu Zhou, and Xia Chen are with the State Key Laboratory of Advanced Electromagnetic Technology and the School of Electrical and Electronic Engineering, Huazhong University of Science and Technology, Wuhan 430074, China (e-mail: yjlin20@foxmail.com; yangqiufan@hust.edu.cn; zhoujianyu87@gmail.com; cxhust@foxmail.com).
Haowen Luo is with the State Grid Jingmen Power Supply Company, Jingmen 448000, China (e-mail: 531298596@qq.com).
Yin Chen (corresponding author) is with the Department of Electronic and Electrical Engineering, University of Strathclyde, Glasgow G1 1XW, UK (e-mail: yin.chen.101@strath.ac.uk).
DOI: 10.23919/PCMP.2023.000164

such as the one proposed in [20]–[22], can help address these issues. However, they may not consider the system network, leading to reduced frequency control accuracy.

Although frequency fluctuations are effectively reduced and power system resiliency is enhanced by these methods, they cannot be easily applied to widespread ES systems directly because of their significant computational burden due to the high dimensionality of the optimization problem. In particular, the entire system is treated as a single bus in the AGC method, and the influence of the grid topology on the frequency dynamics is overlooked. To address these challenges, a partitioning-based control technique is proposed as a potential solution in [8], which involves a partitioning algorithm and a control scheme.

An appropriate partitioning is crucial for improving frequency control accuracy. Network partitioning algorithms have been investigated in several studies over the past decade. In [23], a general fully decentralized partitioning based on peer-to-peer communication is proposed. However, the efficiency of such algorithms may become limited as the scale of the power system increases because of their high computational burden [24]. To overcome this problem, the k-means algorithm is modified in [25] to obtain more accurate partitioning results. However, although the k-means algorithm is widely used for partitioning in other fields, it may not be appropriate for power systems because bus locations in power systems are represented through relative distances in a coordinate system. This poses a challenge for accurately calculating the weights between the buses and the resulting partitions using the k-means algorithm. Moreover, all the aforementioned algorithms require the objectives to be represented in an absolute coordinate system to facilitate centroid calculation and the subsequent provision of the partitioning results based on these centroids. Directly transforming the relative and absolute coordinates can distort the relative information between the buses [26].

There are a few studies on partitioning methods based on relative distances. A novel clustering procedure is performed by utilizing the exchange of distance information between agents and a consensus voting algorithm in [27], whereas a community detection algorithm is used to control drinking water networks in [28]. A community detection algorithm proposed in [29] has been applied in power systems to handle cascading failures in [30], and to control high-voltage transmission networks in [31] and voltage coordination in [32]. Compared to other partitioning methods, this algorithm provides improved partition quality with higher efficiency in large networks [24]. However, the application of community detection algorithms to the control of large-scale ES systems has not been reported in the existing literature.

Partitioning-based control methods for frequency regulation have also been investigated in previous studies. In [8], the Ng–Jordan–Weiss spectral clustering algorithm is proposed to cluster distributed resources into different groups, and distributed model predictive control is utilized to reduce the scale of the control problem by generating the control signal for each group separately. In [33], the k-means algorithm is utilized to regroup heterogeneous loads into distinct homogenous clusters according to their parameters. In [34], EVs are partitioned into three main states and the frequency control signal is dispatched only to EVs in the controllable state. Although the aforementioned network partitioning methods effectively enhance computational efficiency, they fail to recognize the significance of the power system topology in achieving accurate partitioning, which is critical for efficient frequency control. Neglecting the power system topology can potentially lead to suboptimal partitioning and degrade frequency control efficiency.

A comparative summary of frequency control methods for ES systems is presented in Table I. The aggregate model and network structure are neglected in most studies. In contrast, a community detection algorithm based on the electrical distance is adopted in the proposed method in this paper to improve frequency control performance. Frequency control is performed over two layers for aggregating and disaggregating the inertia and droop coefficients to achieve frequency regulation and economical operation. The participation of ES systems in the inertial and primary frequency responses is optimized by considering both frequency regulation and economical operation. The main contributions of this study are as follows.

1) A community detection algorithm-based partitioning method is introduced. Unlike previous studies [23]–[25], partitioning can be performed without determining the number of groups in advance and the partition quality can be directly evaluated.

2) A novel partitioning-based control strategy that incorporates line impedance considerations is introduced to improve frequency control accuracy and stability. In contrast to the control methods in [9]–[11], [13], [22], [33], [34], the proposed strategy accounts for system line impedance and device locations. It is therefore applicable to large-scale power systems.

3) In contrast to centralized control methods [13]–[19], the approach proposed in this study utilizes a distributed control architecture that maintains control performance and stability under a switching communication topology and failures. Global communication is achieved in the distributed architecture through neighboring information exchange, thereby avoiding the single point of failure inherent to centralized control.

The remainder of this paper is organized as follows. Distance measurement and the partitioning algorithm are introduced in Section II. The proposed two-layer frequency control method is presented in Section III. The results of simulations conducted to demonstrate the performance of the proposed method are reported in Section IV. Finally, conclusions are drawn in Section V.

TABLE I
THE COMPARATIVE SUMMARY OF THE LITERATURE REVIEW ON FREQUENCY CONTROL OF ESS

References	Control objectives (besides frequency regulation)	Control methods	Considering aggregate model	Considering network structure	Frequency service type
[8]	Economic operation	Distributed model predictive control	Yes	No	Secondary
[9]	SOC balance	Leader-follower finite-time consensus control	No	No	Secondary
[10]	Battery management	Rule-based BESS Control	No	No	Secondary
[11]	Battery state recovery	Probabilistic control	Yes	No	Secondary
[12]	DC link voltage control	MPC	No	Yes	Secondary
[13]	Active power sharing	Optimization-based disaggregation strategy	Yes	No	Primary
[14]	Power loss minimization	Optimal robust allocation	No	Yes	Primary
[15]–[17]	Converter and generator efforts minimization	H_2 norm optimization	No	Yes	Primary
[18]	Active power sharing	H_2 norm optimization	No	Yes	Primary
[19]	System stability improvement	Multi-step optimization	No	Yes	Primary
[22]	Economic operation	Distributed Quasi-Newton method	No	No	Primary
[33]	Power reduction	Aggregated control scheme	Yes	No	Secondary
[34]	SOC balance	SOC synchronous control	No	No	Secondary
Proposed method	Economic operation	MPC; leader-follower consensus control	Yes	Yes	Primary

II. PARTITIONING ALGORITHM

In this section, the concepts of effective impedance and a community detection algorithm are introduced to lay the foundations for partition quality optimization and frequency control.

A. Distance Measurement

In power systems with many distributed ES systems, the electrical network can be locally aggregated based on their uneven distribution, known as the community structure [35]. Frequency control performance can be affected by the community structure. If line impedance is considered, the considerable differences between the frequency responses of the distributed ES systems in a large-scale power system and the average frequency of the entire system used as the controlled variable may adversely affect frequency regulation performance.

The electrical distance can be effectively dealt with via reasonable partitioning to reduce the frequency variance in each group. The effective impedance, which is directly related to power loss, is therefore a suitable metric for measuring the distances between groups. Using the nodal voltage equation $\boldsymbol{I}=\boldsymbol{Y}\boldsymbol{U}$ and the nodal voltage $\boldsymbol{U}=\boldsymbol{Y}^{-1}(e_k-e_l)$, the effective impedance z_{kl}^{eff} between the buses k and l can be calculated as [36]:

$$z_{kl}^{\text{eff}}=(\boldsymbol{e}_k-\boldsymbol{e}_l)^{\mathrm{T}}\boldsymbol{U}=(\boldsymbol{e}_k-\boldsymbol{e}_l)^{\mathrm{T}}\boldsymbol{Y}^{-1}(\boldsymbol{e}_k-\boldsymbol{e}_l) \tag{1}$$

where $\boldsymbol{Y}$ is the admittance matrix; $\boldsymbol{e}_k$ and $\boldsymbol{e}_l$ denotes a unit vector with 1 at the position index k and l.

B. Partitioning Algorithm

A power network can be viewed as a weighted network with the weights of the edges representing the effective impedances between the buses. The network can be partitioned using a community detection algorithm [33], in which the modularity of a partitioning strategy is calculated as:

$$\rho=\frac{1}{2m}\sum_{i,j}\left(A_{ij}-\frac{k_ik_j}{2m}\right)\delta(c_i,c_j) \tag{2}$$

where

$$\delta(c_i,c_j)=\begin{cases}1, \text{if buses } i \text{ and } j \text{ are in the same group}\\ 0, \text{otherwise}\end{cases} \tag{3}$$

$$\begin{cases}k_i=\sum_j A_{ij}\\ m=\frac{1}{2}\sum_{i,j}A_{ij}\end{cases} \tag{4}$$

$$A_{ij}=1-\frac{z_{ij}^{\text{eff}}}{\max\limits_{i,j} z_{ij}^{\text{eff}}} \tag{5}$$

where ρ is the modularity of the partitioning result; A_{ij} is the electrical weight between buses i and j; k_i is the degree of group i; and m is the total weight of all the edges in the graph. The effective impedance in (1) depends only on the impedance matrix of the power network and the locations of buses i and j. A small effective impedance z_{ij}^{eff} corresponds to a large electrical weight A_{ij} indicating a close connection between the two buses.

From (2), it can be seen that a large value of ρ indicates a favorable partitioning result in which buses between the lines with larger effective impedances are separated into different groups. Consequently, the aim of the partitioning approach is to optimize the value of ρ in the network, which is an NP-hard problem [37]. A heuristic method [24] is introduced to reduce the computational burden.

Suppose each bus belongs to its own group, any two buses can be partitioned in every step, leading to an increment of ρ given by:

$$\Delta\rho_{ij}=\begin{cases}1/(2m)-k_ik_j/(2m)^2, & \text{if } A_{ij}\neq 0\\ 0, & \text{otherwise}\end{cases} \tag{6}$$

In addition, an indirect increment $\Delta\rho'_{jk}$ is also produced by connecting bus k to bus i or bus j, as:

$$\begin{cases}\Delta\rho'_{jk}=\Delta\rho_{ik}+\Delta\rho_{jk}, & \text{if } k \text{ is connected to } i \text{ and } j\\ \Delta\rho'_{jk}=\Delta\rho_{ik}-k_jk_k/m, & \text{if } k \text{ is connected to } i, \text{ not } j\\ \Delta\rho'_{jk}=\Delta\rho_{jk}-k_ik_k/m, & \text{if } k \text{ is connected to } j, \text{ not } i\end{cases} \tag{7}$$

The algorithm can be expressed as follows.

Step 1: Initial condition, i.e., each bus is in its own group. For each bus, e.g., bus i, the initial value of $\Delta\rho_{ij}$ is calculated using (6).

Step 2: The maximum positive $\Delta\rho_{ij}$ is chosen and vertex i is added to the corresponding group j.

Step 3: The weighted network is updated using (7) after Step 2 is carried out in each node.

Step 4: Repeat Steps 2 and 3 until all the buses are partitioned into a group.

After Step 4, the partitioning result with the maximum value of the modularity ρ is selected as the final partitioning result. All the vertices within a close range are then partitioned into groups. The flowchart of the proposed partitioning algorithm is presented in Fig. 1. The proposed two-layer frequency control method is then developed by using this partitioning result and accounting for the electrical distance. This method involves controlling the ES systems within each group and coordinating controls between the groups.

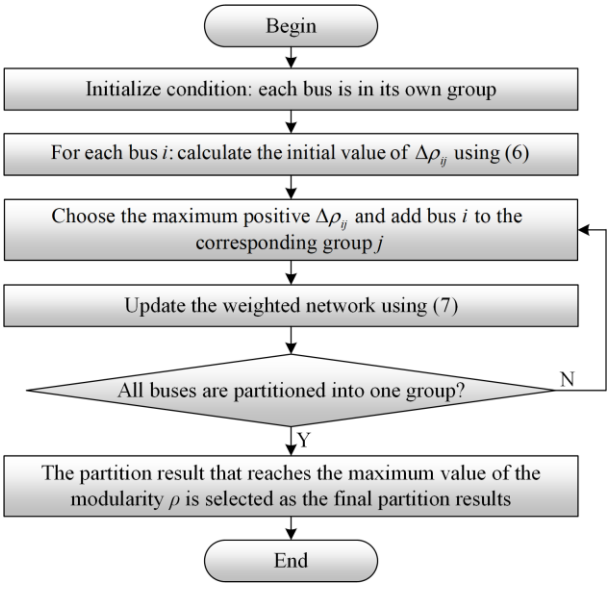

Fig. 1. Flowchart of proposed partitioning algorithm.

III. Two-Layer Frequency Control

In this section, a two-layer frequency control framework inspired by [13] is proposed. The aim of this framework is to achieve the dual objectives of frequency regulation and economical operation. The frequency control scheme consists of two layers: 1) the top layer, which is implemented in a centralized controller, optimizes the total inertia and droop coefficients for favorable frequency regulation performance, and 2) the bottom layer which disaggregates the inertia and droop coefficients for individual ES systems to improve the economic performance of the system.

A. Top Layer Control

As shown in Fig. 2, the controller periodically samples the aggregate information of each group, solves the model predictive control problem, and generates the aggregate inertia and droop coefficients of the groups. The aim of this layer is to improve frequency control for ES systems and maintain the frequency stability of the power system. Virtual inertia serves to emulate the inertial responses of traditional synchronous generators and offer inertial support by renewable energy sources such as solar and wind power. In addition, virtual synchronous machines can regulate and stabilize system frequency by controlling their output power.

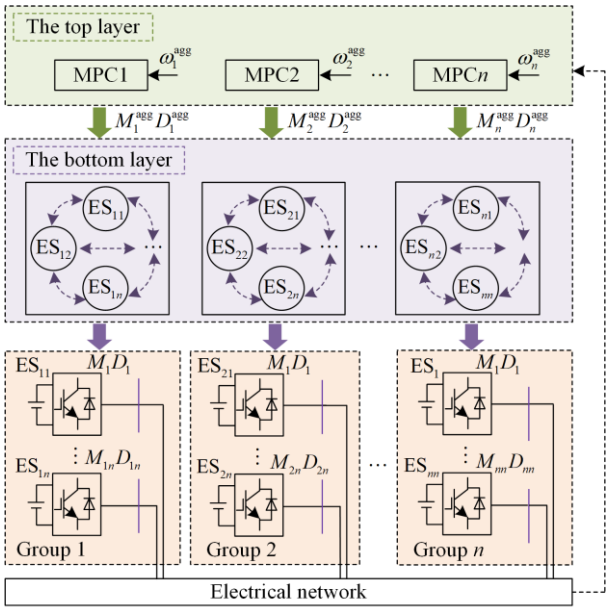

Fig. 2. Block diagram of proposed control scheme.

The frequency dynamics of the entire system, the aggregation process, and the optimization problem, are introduced next.

The power system investigated in this study consists of distributed ES systems, conventional synchronous generators, wind farms, and loads. Inertia and droop controls are adopted in primary control to provide basic power sharing for the ES systems. The frequency dynamics of the ES systems and synchronous generators can be described as:

$$M_g \frac{\mathrm{d}\omega_g}{\mathrm{d}t} = P_g^{\mathrm{m}} - D_g(\omega_g - \omega_{\mathrm{n}}) + P_g - \sum_l P_{gl}, g \in G \quad (8)$$

$$M_i \frac{\mathrm{d}\omega_i}{\mathrm{d}t} = -D_i(\omega_i - \omega_{\mathrm{n}}) + P_i - \sum_j P_{ij}, i \in N_{\mathrm{ES}} \quad (9)$$

$$\tau_g \frac{\mathrm{d}P_g^{\mathrm{m}}}{\mathrm{d}t} = -P_g^{\mathrm{m}} - R_g(\omega_g - \omega_{\mathrm{n}}), g \in G \quad (10)$$

where ω_g, ω_{n}, M_g, and D_g are the generator frequency, synchronous frequency, and the inertia and damping coefficients of the synchronous generator g, respectively; G is the set of conventional generator buses; N_{ES} is the set of ES buses; P_g^{m}, P_g, and P_{gl} are the turbine mechanical power, real power injected at bus g, and real power flow from bus g to l, respectively; M_i and D_i are the inertia and damping coefficients of ES system i, respectively; P_i is the real power injected at the bus of ES system i; τ_g is the time constant of the turbines; and R_g is the inverse of the droop constant.

The inertia coefficient M_g is usually much larger than the turbine time constant τ_g. The latter can therefore be ignored in the aggregate model of each group. The aggregate model of group k is thus expressed as:

$$\frac{\mathrm{d}\omega_k^{\mathrm{agg}}}{\mathrm{d}t} = -\frac{D_k^{\mathrm{agg}}}{M_k^{\mathrm{agg}}}(\omega_k^{\mathrm{agg}} - \omega_{\mathrm{n}}) - \frac{1}{M_k^{\mathrm{agg}}} P_{\mathrm{load},k} \quad (11)$$

where ω_k^{agg} is the average frequency k; $P_{\mathrm{load},k}$ is the aggregate electrical load; while M_k^{agg} and D_k^{agg} are the aggregate inertia and droop coefficients of group k, respectively. The latter three can be calculated as:

$$\begin{cases} M_k^{\mathrm{agg}} = \sum_{g \in G_k} M_g + \sum_{i \in N_{\mathrm{ES}k}} M_i \\ D_k^{\mathrm{agg}} = \sum_{g \in G_k} (D_g + R_g) + \sum_{i \in N_{\mathrm{ES}k}} D_i \\ P_{\mathrm{load},k} = -\sum_{g \in G_k} P_g - \sum_{i \in N_{\mathrm{ES}k}} P_i + \sum_{i \in G_k \cap N_{\mathrm{ES}k}} P_{ij} \end{cases} \quad (12)$$

where G_k and $N_{\mathrm{ES}k}$ are the sets of conventional generators and ES systems that belong to group k, respectively.

The discrete model of (11) can be expressed as:

$$\omega_k^{\mathrm{agg}}(t+1) = \left(1 - \frac{D_k^{\mathrm{agg}}(t)}{M_k^{\mathrm{agg}}(t)} T_{\mathrm{d}}\right) \omega_k^{\mathrm{agg}}(t) + \left(-\frac{1}{M_k^{\mathrm{agg}}(t)} T_{\mathrm{d}}\right) P_{\mathrm{load},k}(t) \quad (13)$$

where T_{d} is the discrete time interval.

The inequality constraints of the state and control variables are expressed as:

$$\begin{cases} \omega_{\min} \leqslant \omega_k(t+1) \leqslant \omega_{\max} \\ M_{\min} \leqslant M_k^{\mathrm{agg}}(t) \leqslant M_{\max} \\ D_{\min} \leqslant D_k^{\mathrm{agg}}(t) \leqslant D_{\max} \end{cases} \quad (14)$$

where $\omega_{\min}$ and $\omega_{\max}$ are the lower and upper bounds of the frequency, respectively; $M_{\min}$ and $M_{\max}$ are the lower and upper bounds of the aggregate inertia coefficients, respectively; $D_{\min}$ and $D_{\max}$ are the lower and upper bounds of the aggregate damping coefficients, respectively. The cost function comprising both the frequency deviation and the inertia and damping coefficients is expressed as:

$$J(t) = \left\|\Delta\boldsymbol{\omega}(t+1)\right\|_{\boldsymbol{Q}}^2 + \left\|\boldsymbol{U}(t)\right\|_{\boldsymbol{R}}^2 = \alpha \sum_{k=1}^{N_{\mathrm{g}}} (\omega_k(t+1) - \omega_{\mathrm{n}})^2 + \beta \sum_{k=0}^{N_{\mathrm{g}}} \left[q(M_k^{\mathrm{agg}}(t))^2 + r(D_k^{\mathrm{agg}}(t))^2 \right] \quad (15)$$

where α, β, q, and r are the weight coefficients of the control objective; $\boldsymbol{Q}$ and $\boldsymbol{R}$ are diagonal matrices composed of coefficients q and r, respectively; the element at position k in the vector $\boldsymbol{U}$(t), which consists of control variables, is [$M_k^{\mathrm{agg}}(t)$, $D_k^{\mathrm{agg}}(t)$].

The control objective is to minimize (15). The obtained control sequence for the current control period, $\boldsymbol{u} = \left[M_1^{\mathrm{agg}}(t), D_1^{\mathrm{agg}}(t), \cdots, M_k^{\mathrm{agg}}(t), D_k^{\mathrm{agg}}(t), \cdots, M_N^{\mathrm{agg}}(t), D_N^{\mathrm{agg}}(t)\right]^{\mathrm{T}}$ is then applied to every group, as shown in Fig. 2.

B. Bottom Layer Control

The aim of the bottom layer is to disaggregate the aggregate inertia and droop coefficients for each ES system to minimize the operating cost of the system. The optimization problem for the optimal response of the ES systems can be expressed as:

$$\min_{M_i^*, D_i^*, i \in N_{\mathrm{ES}k}} \int_{t=0}^{T_{\mathrm{d}}} \sum_{i \in N_{\mathrm{ES}k}} f_i(P_i)\, \mathrm{d}t \quad (16)$$

where the cost function $f_i(\cdot)$ is defined as:

$$f_i(P_i) = a_i(P_i)^2 + b_i P_i + c_i \quad (17)$$

Based on the frequency response of the ES systems in (9), the actual input power P_i provided by ES system i is a function of its inertial and droop coefficients, and can be written as:

$$P_i = P_i^* - M_i^* \Delta \mathrm{d}\omega_k^*(t)/\mathrm{d}t - D_i^* \Delta\omega_k^*(t), i \in N_{\mathrm{ES}k} \quad (18)$$

where P_i^* is the optimal economic dispatch decision for ES system i in group k before the load change; M_i^* is the inertia coefficient of ES system i in group k; D_i^* is its droop coefficient; and $\Delta\omega_k^*$ is the average frequency deviation of group k. Note that the inertia and damping coefficients of the conventional generators are not considered in (16) because the generator parameters cannot be changed.

It is evident that the cost function (17) is strictly convex. Thus, in the steady state, the system operator conducts an economic dispatch to ensure that the increment cost satisfies:

$$f_i'(P_i^*) = -\lambda^*, \forall i \in N_{\mathrm{ES}k} \quad (19)$$

According to (18) and considering

$-M_i^*\Delta \mathrm{d}\omega_k^*(t)/\mathrm{d}t - D_i^*\Delta\omega_k^*(t)$ as a perturbation of P_i^*, the cost function in (17) can be approximated as:

$$\begin{aligned} &f'(P_i^*-M_i^*\Delta \mathrm{d}\omega_k^*(t)/\mathrm{d}t-D_i^*\Delta\omega_k^*(t))\approx f'(P_i^*)+ \\ &f''(P_i^*)M_i^*\Delta \mathrm{d}\omega_k^*(t)/\mathrm{d}t+f''(P_i^*)D_i^*\Delta\omega_k^*(t) \end{aligned} \tag{20}$$

The augmented part in (20) should be kept constant when there is a load change. This yields:

$$\begin{cases} (f''(P_i^*)M_i^* - f''(P_j^*)M_j^*)\Delta \mathrm{d}\omega_k^*(t)/\mathrm{d}t + \\ (f''(P_i^*)D_i^* - f''(P_j^*)D_j^*)\Delta\omega_k^*(t) = 0 \\ \forall i,j \in N_{\mathrm{ES}k} \end{cases} \tag{21}$$

As this constraint must hold for any value of $\Delta \mathrm{d}\omega_k^*(t)/\mathrm{d}t$ and $\Delta\omega^*(t)$ $(\forall t \geqslant 0)$, the following conditions hold:

$$\begin{cases} f''(P_i^*)M_i^* = f''(P_j^*)M_j^* \\ f''(P_i^*)D_i^* = f''(P_j^*)D_j^* \end{cases}, \forall i,j \in N_{\mathrm{ES}k} \tag{22}$$

Thus, the optimal inertia and damping coefficients for all the ES systems belonging to group *k* are given by:

$$\begin{cases} M_i^* = \dfrac{M_k^{\mathrm{agg}}(t) - \sum_{g\in G_k} M_g}{f''(P_i^*)\sum_{j\in N_{\mathrm{ES}k}} (f''(P_j^*))^{-1}} \\ D_i^* = \dfrac{D_k^{\mathrm{agg}}(t) - \sum_{g\in G_k} (D_G + R_G)}{f''(P_i^*)\sum_{j\in N_{\mathrm{ES}k}} (f''(P_j^*))^{-1}} \end{cases}, \forall i \in N_{\mathrm{ES}k} \tag{23}$$

Using (23), the control parameters M_i^* and D_i^* can be directly calculated and sent to each ES controller in the centralized mode. The computational speed of the proposed model and techniques is comparable to that of a single-droop control approach. Thus, the optimization process involved in determining the optimal values of the inertia and droop coefficients can be efficiently completed within the time frame required for frequency regulation. Therefore, the proposed model and techniques can be executed with sufficient speed for effective frequency regulation.

However, centralized control requires all the ES systems to be linked to a centralized controller in which all the required information, such as the network and load parameters, is collected to solve the control problem and control each ES. This approach typically suffers from a long computation time, considerable communication overhead, privacy issues, and low scalability. In contrast, distributed control requires no centralized controller. Instead, the system converges to an optimal solution through neighbor-to-neighbor communication over a sparse communication network, which is more appropriate for widely distributed ES systems. The modeling and design of the distributed control algorithm to maintain (22) in distributed mode is thus introduced next.

Communication between the ES systems can be described by an undirected graph $G := \{V, E\}$ of the set of all the ES systems $V := \{V_1, V_2, \cdots, V_N\}$ and the set of communication links $E \subseteq V \times V$. If nodes *i* and *j* have a communication link, then $(V_i, V_j) \in E$. The Laplace matrix $\boldsymbol{L} \in \boldsymbol{R}^{N\times N}$ is defined as:

$$\boldsymbol{L} = [l_{ij}] = \begin{cases} \sum_{j=1}^{N} a_{ij}, i = j \\ -a_{ij}, i \neq j \end{cases} \tag{24}$$

where a_{ij} denotes the communication weight, and it is a positive value if $(V_i, V_j) \in E$ and 0 otherwise.

For a system with a leader (labeled as node 1), the pinning gain is defined as:

$$\begin{cases} g_i > 0, \exists (V_i, V_1) \\ g_i = 0, \text{otherwise} \end{cases} \tag{25}$$

A leader-follower consensus algorithm is proposed to allocate the control signals $M_1^{\mathrm{agg}}(t)$ and $D_1^{\mathrm{agg}}(t)$ from the upper layer to each ES system, as shown in Fig. 2. To maintain (22), the local state variables of the ES system are defined as follows:

$$\begin{cases} \gamma_i^{\mathrm{M}} = f''(P_i^*)M_i^* = h_i M_i^* \\ \gamma_i^{\mathrm{D}} = f''(P_i^*)D_i^* = h_i D_i^* \end{cases} \tag{26}$$

where γ_i^{M} and γ_i^{D} are local state variables of the inertia and droop coefficients.

The number of leader is set to 1. The leader can receive control signals from the upper layer to update its inertia and droop coefficients M_1^* and D_1^* as follows:

$$\begin{cases} M_1^* = \dfrac{M_k^{\mathrm{agg}}(t) - \sum_{g\in G_k} M_g}{|N_{\mathrm{ES}k}|} \\ D_1^* = \dfrac{D_k^{\mathrm{agg}}(t) - \sum_{g\in G_k} (D_G + R_G)}{|N_{\mathrm{ES}k}|} \end{cases} \tag{27}$$

where M_k^{agg} and D_k^{agg} are the aggregate inertia and droop coefficients for group *k* from the top layer, respectively; while $|N_{\mathrm{ES}k}|$ is the cardinality of $N_{\mathrm{ES}k}$.

The dynamics of the inertia and droop coefficients of the followers are as follows:

$$\begin{cases} \dfrac{\mathrm{d}M_i^*}{\mathrm{d}t} = u_i^{\mathrm{M}} \\ \dfrac{\mathrm{d}D_i^*}{\mathrm{d}t} = u_i^{\mathrm{D}} \end{cases} \tag{28}$$

where

$$\begin{cases} u_i^{\mathrm{M}} = \sum_j a_{ij}(\gamma_i^{\mathrm{M}} - \gamma_j^{\mathrm{M}}) - g_{k,i}(\gamma_i^{\mathrm{M}} - \gamma_1^{\mathrm{M}}) \\ u_i^{\mathrm{D}} = \sum_j a_{ij}(\gamma_i^{\mathrm{D}} - \gamma_j^{\mathrm{D}}) - g_{k,i}(\gamma_i^{\mathrm{D}} - \gamma_1^{\mathrm{D}}) \end{cases} \tag{29}$$

Let $\hat{\gamma}_i = \gamma_i - \gamma_1 = h_i M_i^* - h_1 M_1^*$, equation (29) can then be rewritten as:

$$\begin{cases} u_i^{\mathrm{M}} = \sum_j a_{ij}(\hat{\gamma}_i^{\mathrm{M}} - \hat{\gamma}_j^{\mathrm{M}}) - g_{k,i}\hat{\gamma}_i^{\mathrm{M}} \\ u_i^{\mathrm{D}} = \sum_j a_{ij}(\hat{\gamma}_i^{\mathrm{D}} - \hat{\gamma}_j^{\mathrm{D}}) - g_{k,i}\hat{\gamma}_i^{\mathrm{D}} \end{cases} \tag{30}$$

Because the steady-state values of the derivatives of the inertia and droop coefficients are zero, the steady state of (30) can be expressed as:

$$\begin{cases} \dfrac{\mathrm{d}\boldsymbol{M}^{\mathrm{ss}}}{\mathrm{d}t} = \boldsymbol{0} = (\boldsymbol{L}+\boldsymbol{G})\hat{\gamma}^{\mathrm{M,ss}} \Rightarrow \hat{\gamma}^{\mathrm{M,ss}} = (\boldsymbol{L}+\boldsymbol{G})^{-1}\boldsymbol{0} = \boldsymbol{0} \\ \dfrac{\mathrm{d}\boldsymbol{D}^{\mathrm{ss}}}{\mathrm{d}t} = \boldsymbol{0} = (\boldsymbol{L}+\boldsymbol{G})\hat{\gamma}^{\mathrm{D,ss}} \Rightarrow \hat{\gamma}^{\mathrm{D,ss}} = (\boldsymbol{L}+\boldsymbol{G})^{-1}\boldsymbol{0} = \boldsymbol{0} \end{cases} \tag{31}$$

where the superscript "ss" in $\hat{\gamma}^{\mathrm{M,ss}}$ and $\hat{\gamma}^{\mathrm{D,ss}}$ stands for the steady state.

Equation (31) implies that:

$$\begin{cases} \lim\limits_{t\to\infty}\left\|\gamma_i^{\mathrm{M}}(t)-\gamma_1^{\mathrm{M}}(t)\right\| = 0, \forall i = 2,\cdots,\left|N_{\mathrm{ES}k}\right| \\ \lim\limits_{t\to\infty}\left\|\gamma_i^{\mathrm{D}}(t)-\gamma_1^{\mathrm{D}}(t)\right\| = 0, \forall i = 2,\cdots,\left|N_{\mathrm{ES}k}\right| \end{cases} \tag{32}$$

which in turn implies that the consensus of the system can be achieved as:

$$\begin{cases} \lim\limits_{t\to\infty}\left\|f''(P_i^*)M_i^*(t)-f''(P_1^*)M_1^*(t)\right\|=0, \forall i=2,\cdots,\left|N_{\mathrm{ES}k}\right| \\ \lim\limits_{t\to\infty}\left\|f''(P_i^*)D_i^*(t)-f''(P_1^*)D_1^*(t)\right\|=0, \forall i=2,\cdots,\left|N_{\mathrm{ES}k}\right| \end{cases} \tag{33}$$

Equation (22) is hence maintained in distributed mode, thereby guaranteeing high resilience and efficiency.

IV. Simulation Results

Four simulation cases are designed to compare the proposed method with other control methods. The effectiveness of the proposed partitioning method is verified in subsection A. In subsections B and C, the basic control performance of the proposed control method is compared with those of existing control methods. In subsection E, the verification of the plug-and-play functionality of the proposed control approach is presented.

The proposed method is evaluated in an IEEE 39-bus network with ES systems labelled as ES1–ES12 randomly installed in buses 4, 6, 13, 16, 18, 19, 23, 26, 30, 31, 35, and 37, as shown in Fig. 3. The impedance parameters and conventional loads of the system are set to those of the IEEE 39-bus and the base power is set to 100 MVA. The parameters of the conventional generators are listed in Table II. The comprehensive details of the control algorithm are listed in Table III, whereas Table IV lists the parameters associated with the ES systems. The cost coefficients a_i and b_i are modeled as truncated Gaussian distributions (μ, σ^2). Matlab is used to execute the partitioning algorithm presented in Section II, while the control algorithm and frequency regulation model explained in Section III are realized using the simulink framework. The partitioning algorithm is incorporated into the control algorithm by leveraging the functionality of the Matlab function block, which is a robust tool for seamlessly integrating custom algorithms into the simulink environment.

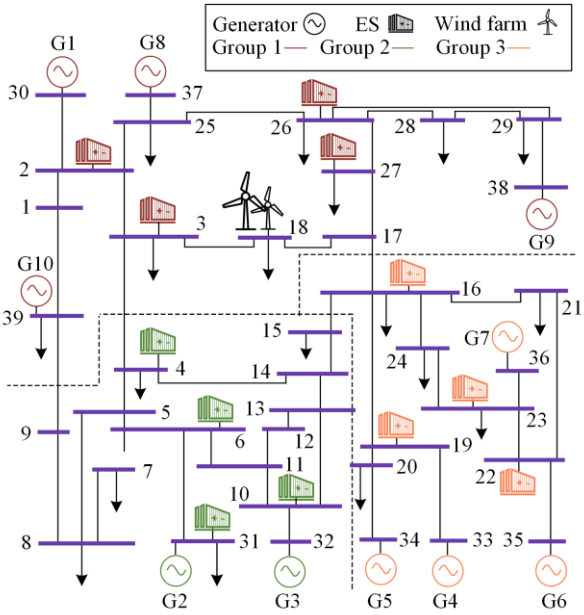

Fig. 3. Schematic diagram of test network and partitioning result by proposed method.

TABLE II
Parameters of the Test Network

Parameters	Value
R (p.u.)	[2.5, 5.7, 6.5, 6.3, 5.1, 6.5, 5.6, 5.4, 8.3, 10]
τ_g (s)	[4, 5, 6, 4.5, 5, 5.5, 5, 4.5, 5, 6]
M_{G} (p.u.)	[42, 30.3, 35.8, 28.6, 26, 34.8, 26.4, 24.3, 34.5, 500]
D_{G} (p.u.)	1.5
S_{base} (MVA)	100
ω_{ref} (Hz)	50

TABLE III
Parameters of the MPC and Consensus Algorithm

Parameters	Value
a_{ij}	0.5
g_i	1.2
q/r	1/1
T_{d} (s)	1
$\omega_{\max}/\omega_{\min}$ (p.u.)	±0.01

TABLE IV
Parameters of the ES Systems

Parameters	Value
S_{base} (MVA)	100
$M_{\max}/M_{\min}$ (p.u.)	30/10
$D_{\max}/D_{\min}$ (p.u.)	20/10
C_{i} (MWh)	3.2
$SOC_{\max}/SOC_{\min}$	0.8/0.2
$SOC(0)$	0.5
a_i	$(2.7,1.5^2)$, no less than 0.5
b_i	$(60, 15^2)$, no less than 10
c_i	0
a/β	0.9/0.1

A. Comparison of Partitioning Results

To verify the effectiveness and influence of the proposed partitioning method on frequency control, a comparative study of different partitioning methods is presented. At t=2 s, the loads at buses 18, 19, and 31 undergo a step increase of 0.1 p.u. The root mean squared error (RMSE) of the frequency is utilized to measure the effectiveness of frequency control. A lower ω_{RMSE} indicates a better partitioning result, while ω_{RMSE} for the different partitioning results are calculated as:

$$\omega_{\text{RMSE}} = \frac{1}{T}\int_0^T \sqrt{\frac{1}{|B|}\sum_{i\in B}(\omega_i - \omega_{\text{ref}})^2}\,\mathrm{d}t \tag{34}$$

where B denotes the set of buses; ω_i is the frequency of bus i after control following the disturbance; ω_{ref} the frequency before the disturbance; and $|\cdot|$ means the cardinality of the set.

The partitioning results from two other methods in existing papers are presented along with those from the proposed method in Table V. The ω_{RMSE} values and modularity ρ are also listed to compare the partition quality. As shown in Fig. 4, under the step load in bus 17, the proposed method achieves better performance compared with the other methods by partitioning the ES systems with similar frequency characteristics into the same group. This case study shows that the proposed method partitions the network with higher modularity, and enhances coupling within each group and decoupling between different groups.

Based on the partitioning results from the proposed method, ES systems 1, 2, 3, and 10 are partitioned into Group 1; 4, 6, 7, and 11 into Group 2; and 5, 8, 9, and 12 into Group 3. The ES systems are renamed as $\text{ES}_{1\text{-}1}$ to $\text{ES}_{1\text{-}4}$, $\text{ES}_{2\text{-}1}$ to $\text{ES}_{2\text{-}4}$, and $\text{ES}_{3\text{-}1}$ to $\text{ES}_{3\text{-}4}$. The final partitioned groups are shown in different colors in Fig. 3.

TABLE V
THE COMPARISON OF DIFFERENT CONTROL METHODS

Methods		I (Method in [13])	II	III (Conventional droop control)	IV	Proposed method
Functions	Economic dispatch	√	√	×	×	√
	Partitioning algorithm	×	×	√	√	√
	Dynamically adjustment of M_d / D_d	×	√	×	√	√
Frequency control performance	ω_{RMSE} (Hz)	0.0643	0.0663	0.0607	0.0595	0.0613
	ω_{nadir} (Hz)	0.0951	0.0921	0.0816	0.0805	0.0825
	ω_{ss} (Hz)	0.0570	0.0694	0.0558	0.0550	0.0567
Operational cost ($)		4.404	4.417	4.417	5.625	4.426
Information required	Generator parameters	√	√	√	√	√
	System frequency	×	√	×	√	√
	Load power	√	√	√	√	√
	Operation cost coefficient	√	√	×	×	√

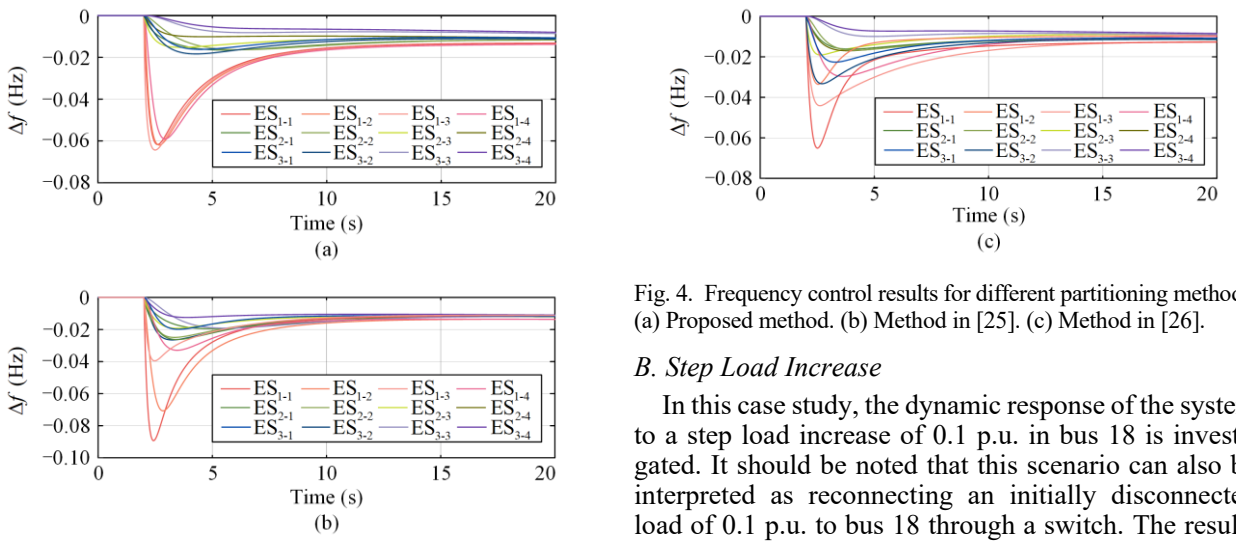

Fig. 4. Frequency control results for different partitioning methods. (a) Proposed method. (b) Method in [25]. (c) Method in [26].

B. Step Load Increase

In this case study, the dynamic response of the system to a step load increase of 0.1 p.u. in bus 18 is investigated. It should be noted that this scenario can also be interpreted as reconnecting an initially disconnected load of 0.1 p.u. to bus 18 through a switch. The results

from the different control methods are listed in Table V. Method I corresponds to the method in [13] where the total inertia and droop coefficients of the ES systems are fixed to $\sum_{i\in N_{ES}} D_i = 43.07$ and $\sum_{i\in N_{ES}} M_i = 61.44$ to ensure $|\omega_{nadir}| \leqslant 0.1$ Hz. In Method II, the partitioning algorithm in Section II.B is omitted, i.e., the number of groups is set to 1, while the proposed method utilizes three groups. In Method III, the inertia and droop coefficients of all the ES systems are fixed and the operating cost of the system is not considered. In Method IV, the total inertia and droop coefficients of the groups are tuned dynamically in a similar manner to the proposed method but the operating cost is not considered. Control targets comprising frequency RMSE (ω_{RMSE}), frequency nadir (ω_{nadir}), and steady-state deviation (ω_{ss}) are compared.

The simulation results for the system frequency deviations under the different control methods are shown in Fig. 5(a). The green and blue trajectories correspond to Methods I and II, respectively, while the frequency response of the proposed method is shown as the red trace. As seen, the proposed method outperforms Methods I and II in effectively suppressing the frequency nadir ω_{nadir} and eliminating oscillations. The superior control performance of the proposed method can be attributed to the following reasons:

1) The inertia and damping coefficients are dynamically adjusted by solving (15) using the real-time information of the power system, such as the frequency and load power. The profiles of the inertia and droop coefficients are presented in Fig. 6.

2) The ES systems are partitioned into groups to improve the frequency response.

The operating costs of the different control methods are compared in Fig. 5(b). The operating cost of Method III, in which the inertia and droop coefficients of all the ES systems are fixed and identical, is shown in blue, while the green line denotes the operating cost of Method IV, in which the total inertia and droop coefficients of the groups are tuned dynamically at set intervals (1 s in this case) to solve (15) and the ES parameters are equally allocated. The red line represents the proposed method. The difference between the red and green lines is that the control parameters for the ES systems in the former are given by (22) to minimize the operating cost. The results show that the proposed method can significantly improve the economic performance of the system compared to the other methods.

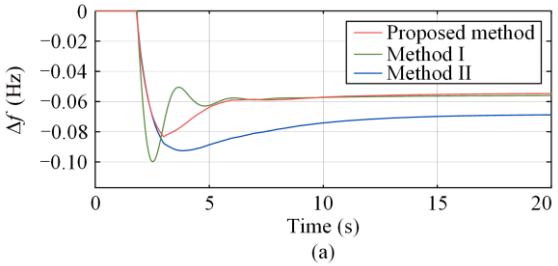

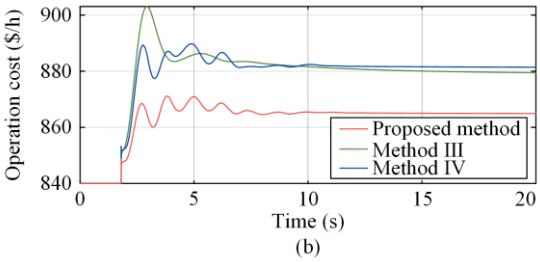

Fig. 5. Simulation results for step load increase condition. (a) System frequency. (b) Operating cost.

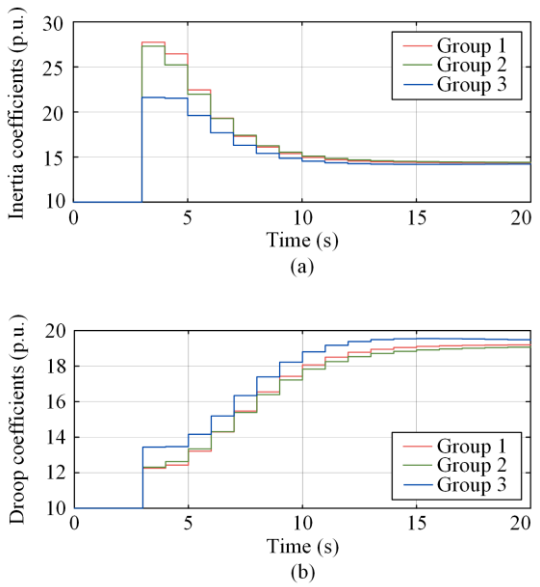

Fig. 6. Control signals of the proposed method under step load increase condition. (a) Inertia coefficients. (b) Droop coefficients.

C. Normal Operation

The dynamic performance of the proposed method is further studied by adding wind power to bus 18 of the system, as shown in Fig. 3. The wind power is shown in Fig. 7. The simulation results presented in Fig. 8 show that compared with the other methods, the proposed method provides clearly improved frequency control at a comparable operating cost. The inertia and droop coefficient profiles are shown in Fig. 9.

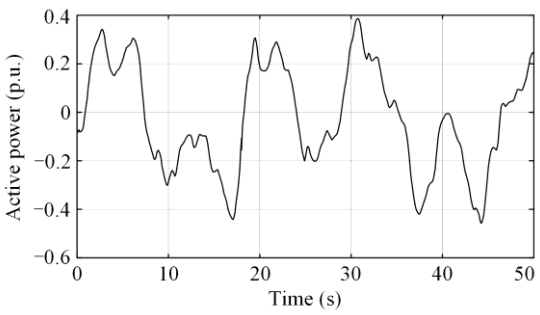

Fig. 7. Active power of wind farm (the base power is set to 100 MVA).

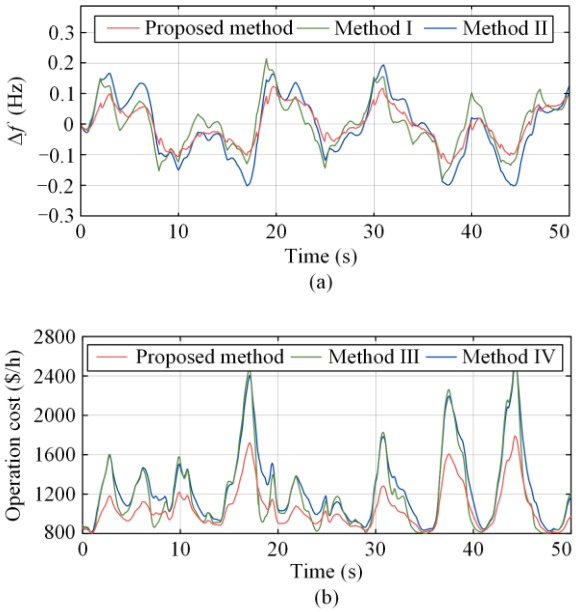

Fig. 8. Simulation results for normal operation condition. (a) System frequency. (b) Operating cost.

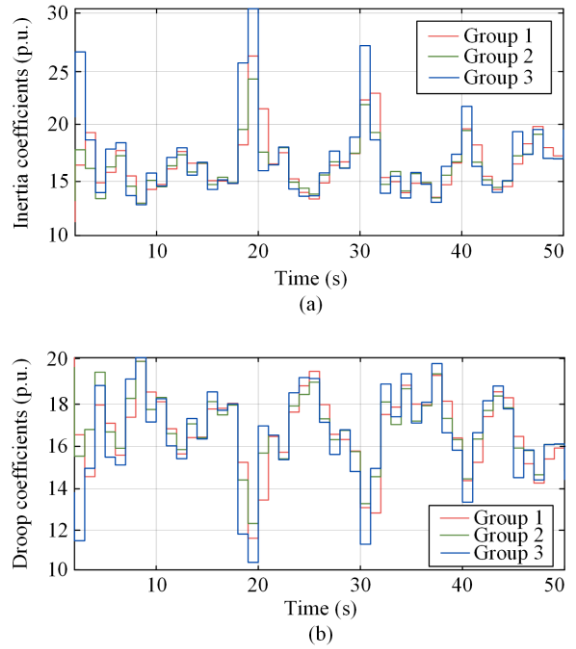

Fig. 9. Control signals of proposed method under normal operation condition. (a) Inertia coefficients. (b) Droop coefficients.

The following conclusions can be drawn from the comparisons:

1) Compared to Methods I and III, the inertia and droop coefficients are dynamically adjusted in the proposed methodbased on real-time information of the power system, such as the frequency and load power. As a result, the proposed method is able to effectively suppress frequency regulation targets such as ω_{nadir} and ω_{ss}, leading to the elimination of oscillations.

2) Compared with Method II, frequency regulation is improved by ES partitioning, which is a key feature of the proposed method. Line impedance can cause significant variations in the frequency responses of distributed ES systems in a large-scale power system. Therefore, simply using the average frequency of the entire system as a controlled variable, as in Method II, may result in poor control performance. In comparison, proper partitioning can effectively account for the electrical distances and reduce the frequency variation within each group, leading to better control performance.

3) Compared with Method IV, the proposed approach considers both primary frequency regulation and economic performance in the power system. As a result, the frequency control requirement is satisfied while the overall system operating cost is reduced. In contrast, Method IV focuses only on frequency regulation without considering the economic aspect, leading to suboptimal cost performance.

D. Operation Under Another Type of Wind Power Disturbance

The dynamic performance of the system under wind power output disturbances with longer timescales and more extreme operating conditions is investigated in this subsection, to highlight the effectiveness of the proposed control algorithm in addressing severe wind power disturbances. Similar to the previous subsection, wind power is added to bus 18 of the system, but with a different output sequence of 300 s obtained from [38], as shown in Fig. 10. It should be noted that the wind power disturbances in Fig. 10 represent the deviations from the steady-state wind power, as forecasted earlier, rather than the actual outputs.

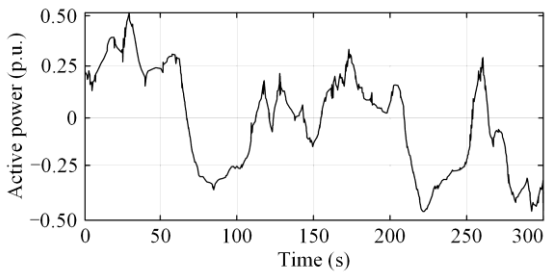

Fig. 10. A second type of wind power disturbance (the base power is set to 100 MVA).

Figure 11 shows the superiority of the proposed method for frequency control and economical operation under prolonged wind power disturbances. The variations of the inertia and droop coefficients with time are shown in Fig. 12. Because of the larger unpredictability of wind power, more frequent fluctuations are present in the inertia and droop coefficients compared to those in Section IV.C. However, these variations consistently remain within the operational constraints without endangering system safety.

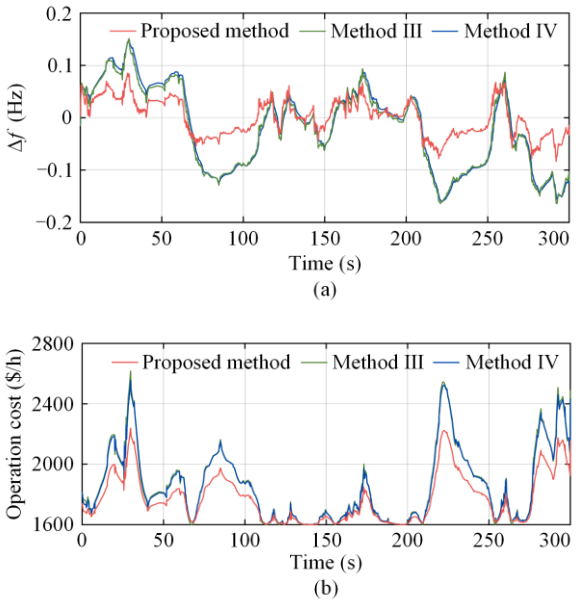

Fig. 11. Simulation results for operation under second type of wind power disturbance. (a) System frequency. (b) Operating cost.

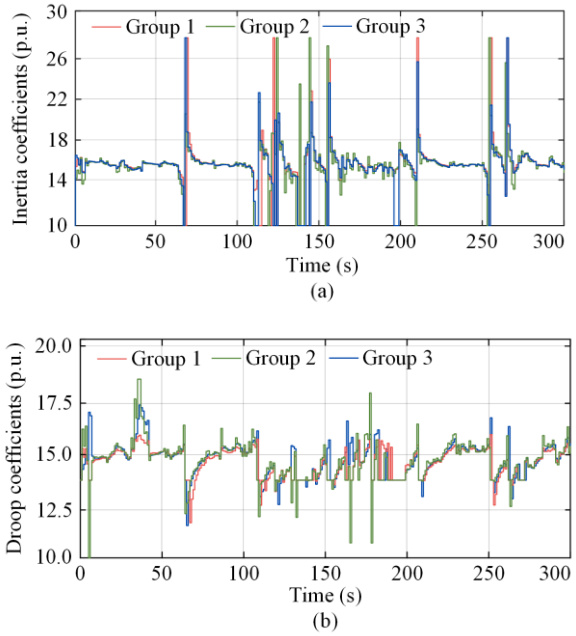

Fig. 12. Control signals for operation under second type of wind power disturbance. (a) Inertia coefficients. (b) Droop coefficients.

E. Communication Topology Switching

The control performance under communication topology switching is also evaluated to illustrate the resilience and flexibility of the proposed control method. The topology switching and corresponding system responses are shown in Fig. 13. The communication links between ES 4 and the other ES systems are completely severed at t=50 s to simulate a scenario similar to the shutdown of an ES unit. By analyzing this specific scenario, the resilience and effectiveness of the ES systems in maintaining system performance during communication disruptions can be evaluated. At the beginning, the frequency deviation at the steady state is limited to less than 0.15 Hz with the communication links intact. At t=25 s, the 1–4 communication link is broken although the topology remains connected. As shown in Fig. 13(a), the steady-state frequency deviation is maintained at nearly the same value and there is no persistent impact under the proposed frequency control method. As seen from Figs. 13(b) and (c), the inertia and droop coefficients of the ES controllers remain constant even after the link failure. At t=50 s, the switching topology is unbalanced by the failure of the 3–4 link, which causes ES 4 to be isolated from the other ES systems in the same group. However, the control objective is maintained because the other ES systems share the inertia and droop coefficients originally allocated to ES 4. Finally, at t=75 s, ES 4 is returned to service immediately after the recovery of the 1–4 link. This demonstrates the resilience of the proposed control method under switching communication topologies and its ability to maintain stability during communication failure.

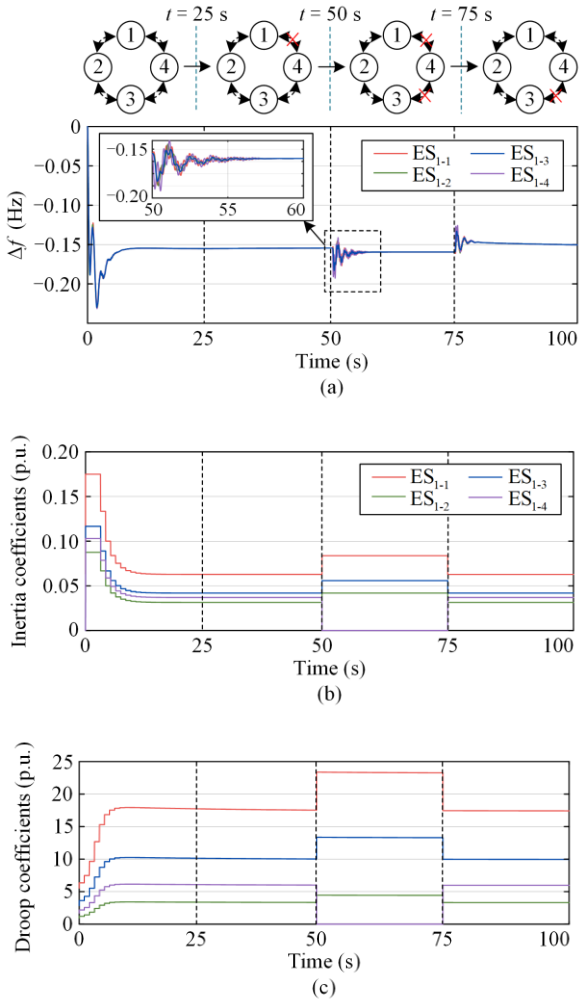

Fig. 13. Simulation results for switching communication topology condition. (a) System frequency. (b) Inertia coefficients. (c) Droop coefficients.

F. Comparison of Computational Time

As shown in (23), the computational complexity of the developed model is equivalent to that of single-droop control but with a faster computational speed. To highlight the difference in computational time, a comparison is performed between the proposed algorithm and a traditional algorithm.

In the traditional algorithm for comparison, equation (15) is used as the objective function for the top layer optimization problem and (16) as the objective function for the bottom layer optimization problem. The top layer optimization problem can therefore be formulated mathematically as:

$$\min (15),\ \text{s.t. } (8)-(14) \tag{35}$$

The bottom layer optimization problem can be expressed mathematically as:

$$\min (16),\ \text{s.t.} \begin{cases} (17)-(18) \\ \sum_{i\in N_{\mathrm{ES}k}} M_i^*/D_i^* = M_k^{\mathrm{agg}}/D_k^{\mathrm{agg}} \\ M_{\min}^* \leqslant M_i^* \leqslant M_{\max}^* \\ D_{\min}^* \leqslant D_i^* \leqslant D_{\max}^* \end{cases} ,i \in N_{\mathrm{ES}k} \tag{36}$$

The Matlab distributed optimization toolbox and the Cholesky factorization algorithm are used to address this quadratic convex optimization problem within the distributed solution environment. The solution times of the proposed control method based on distributed consensus and the traditional method for two systems of different scales are compared in Table VI.

TABLE VI
SOLVING TIME

System	Proposed method (s)	Traditional algorithm (s)
3 Groups, each containing 12 ES systems	0.016 097	0.688 76
3 Groups, each containing 100 ES systems	0.492 79	70.1583

As seen, both methods can meet the control timescale requirement of a solution time of less than 1 s when the number of controlled ES systems is small (corresponding to a scenario of three groups, each containing 12 ES systems). However, with a larger number of controlled ES systems, the solution time of traditional optimization algorithms is significantly increased, making them impractical. Therefore, the proposed method is better suited for handling situations requiring control of a large number of ES systems.

V. CONCLUSION

In this study, a partitioning-based frequency control method using a community detection algorithm partitioning method has been proposed for ES systems. The proposed method optimizes both the inertial and primary frequency responses of ES systems to achieve effective frequency regulation and economical operation. Simulations on a modified IEEE 39-bus system demonstrate that the proposed method achieves effective frequency regulation and economical operation, and outperforms other methods in terms of frequency deviation and total cost. The results highlight the importance of considering the power system topology in partitioning-based methods and showcase the resilience and flexibility of the proposed method in handling unexpected circumstances through a distributed framework.

The proposed method provides a promising solution for frequency regulation and economical operation of power systems with ES systems, which can potentially enhance the reliability, efficiency, and sustainability of power systems. This approach provides a practical solution to overcome the challenges associated with power systems containing widely distributed ES systems.

ACKNOWLEDGMENT

Not applicable.

AUTHORS' CONTRIBUTIONS

Yujun Lin: conceptualization, methodology, software, and writing-original draft. Haowen Luo: investigation, data curation. Yin Chen: writing-reviewing and editing, and supervision. Qiufan Yang: validation and visualization. Jianyu Zhou: methodology and supervision. Xia Chen: methodology, writing- reviewing and editing. All authors read and approved the final manuscript.

FUNDING

This work is supported by the State Key Laboratory of Power System Operation and Control.

AVAILABILITY OF DATA AND MATERIALS

Please contact the corresponding author for data material request.

DECLARATIONS

Competing interests: The authors declare that they have no known competing financial interests or personal relationships that could have appeared to influence the work reported in this article.

AUTHORS' INFORMATION

Yujun Lin received the B.S. degrees in electrical engineering from Chongqing University, Chongqing, China, in 2020. He is currently working toward his Ph.D. degree in electrical engineering at Huazhong University of Science and Technology (HUST), Wuhan, China. His

research interests include the distributed control and optimization of energy storage clusters.

Haowen Luo received the B.S. degrees in power system and automation from Hubei University of Technology, Wuhan, China, in 2013. He is currently working at State Grid Jingmen Power Supply Company, Jingmen, China. His research interests include the renewable energy, energy storage, relay protection and control.

Yin Chen received the B.S. degree in electrical engineering from the Huazhong University of Science and Technology, Wuhan, China, in 2009, the M.S. degree in electrical engineering from Zhejiang University, Hangzhou, China, in 2014, and the Ph.D. degree in electrical engineering from the University of Strathclyde, Glasgow, U.K., in 2020. He is currently a postdoctoral researcher with the University of Strathclyde. His research interests include the modeling of power electronic converters, grid integration of renewable power, and stability analysis of the HVDC transmission systems.

Qiufan Yang received the B.S. degrees in electrical engineering from Huazhong University of Science and Technology (HUST), Wuhan, China, in 2019. He is currently working toward his Ph.D. degree in electrical engineering at HUST, Wuhan, China. His current research interests include microgrids, distributed control, and energy storage control technology.

Jianyu Zhou received the B.S. degree in electrical engineering from the Huazhong University of Science and Technology, Wuhan, China, where he is currently working toward the Ph.D. degree in electrical engineering. His research interests include dc microgrids, distributed control, and hybrid energy storage.

Xia Chen received the B.S. degree in power system and its automaton from the Wuhan University of Technology, Wuhan, China, in 2006, and the M.S. and Ph.D. degrees in electrical engineering from the Huazhong University of Science and Technology (HUST), Wuhan, China, in 2008 and 2012, respectively. From 2012 to 2015, she was a postdoctoral research fellow with the University of Hong Kong, Hong Kong. In 2015, she joined the HUST and is currently a professor with the School of Electrical and Electronic Engineering, HUST. Her research interests include distributed control technology in microgrid, renewable energy integration technologies, and new smart grid device.

REFERENCES

[1] X. Chen, Y. Liu, and Q. Wang *et al*., "Pathway toward carbon-neutral electrical systems in China by mid-century with negative CO_2 abatement costs informed by high-resolution modeling," *Joule*, vol. 5, no. 10, pp. 2715-2741, Oct. 2021.

[2] N. Samaan, M. A. Elizondo, and B. Vyakaranam *et al*., "Combined transmission and distribution test system to study high penetration of distributed solar generation," in *2018 IEEE/PES Transmission and Distribution Conference and Exposition* (*T&D*), Denver, USA, Apr. 2018, pp. 1-5.

[3] Q. Nguyen, H. V. Padullaparti, and K. Lao *et al*., "Exact optimal power dispatch in unbalanced distribution systems with high PV penetration," *IEEE Transactions on Power Systems*, vol. 34, no. 1, pp. 718-728, Jan. 2019.

[4] L. Shang, X. Dong, and C. Liu *et al*., "Fast grid frequency and voltage control of battery energy storage system based on the amplitude-phase-locked-loop," *IEEE Transactions on Smart Grid*, vol.13, no.2, pp. 941-953, Dec. 2021.

[5] Y. Chen, L. Xu, and A. Egea-Àlvarez *et al*., "MMC impedance modeling and interaction of converters in close proximity," *IEEE Journal of Emerging and Selected Topics in Power Electronics*, vol. 9, no. 6, pp. 7223-7236, Dec. 2021.

[6] L. Meng, J. Zafar, and S. K. Khadem *et al*., "Fast frequency response from energy storage systems—a review of grid standards, projects and technical issues," *IEEE Transactions on Smart Grid*, vol. 11, pp. 1566-1581, Oct. 2019.

[7] D. A. Kez, A. M. Foley, and D. J. Morrow, "Analysis of fast frequency response allocations in power systems with high system non-synchronous penetrations," *IEEE Transactions on Industry Applications*, vol. 58, pp. 3087-3101, Mar. 2022.

[8] Z. Yi, Y. Xu, and W. Gu *et al*., "Distributed model predictive control based secondary frequency regulation for a microgrid with massive distributed resources," *IEEE Transactions on Sustainable Energy*, vol. 12, pp. 1078-1089, Oct. 2020.

[9] Y. Wang, Y. Xu, and Y. Tang *et al.*, "Aggregated energy storage for power system frequency control: a finite-time consensus approach," *IEEE Transactions on Smart Grid*, vol. 10, pp. 3675-3686, May 2018.

[10] S. Chen, T. Zhang, and H. B. Gooi *et al*., "Penetration rate and effectiveness studies of aggregated BESS for frequency regulation," *IEEE Transactions on Smart Grid*, vol. 7, pp. 167-177, Jun. 2015.

[11] M. Wang, Y. Mu, and Q. Shi *et al*., "Electric vehicle aggregator modeling and control for frequency regulation considering progressive state recovery," *IEEE Transactions on Smart Grid*, vol. 11, pp. 4176-4189, Mar. 2020.

[12] L. Subramanian, V. Debusschere, and H. B. Gooi *et al*., "A distributed model predictive control framework for grid-friendly distributed energy resources," *IEEE Transactions on Sustainable Energy*, vol. 12, pp. 727-738, Aug. 2020.

[13] S. S. Guggilam, C. Zhao, and E. Dall'Anese *et al*., "Optimizing DER participation in inertial and primary-frequency response," *IEEE Transactions on Power Systems*, vol. 33, no.1, pp. 5194-5205, Jan. 2018.

[14] B. K. Poolla, S. Bolognani and F. Dorfler, "Optimal placement of virtual inertia in power grids," *IEEE Transactions on Automatic Control*, vol. 62, pp. 6209-6220, May 2017.

[15] F. Paganini and E. Mallada, "Global analysis of synchronization performance for power systems: bridging the theory-practice gap," *IEEE Transactions on Automatic Control*, vol. 65, pp. 3007-3022, Sept. 2019.

[16] Y. Jiang, R. Pates and E. Mallada, "Dynamic droop control in low-inertia power systems," *IEEE Transactions on Automatic Control*, vol. 66, pp. 3518-3533, Oct. 2020.

[17] J. Liu, S. Zhu, and P. Liu *et al*., "Coordinated control strategy for wind turbine and energy storage equipment considering system frequency safety and stability constraints," *Power System Protection and Control*, vol. 52, pp. 73-84, Jan. 2024. (in Chinese)

[18] G. S. Misyris, A. Tosatto, and S. Chatzivasileiadis *et al*., "Zero-inertia offshore grids: N-1 security and active power sharing," *IEEE Transactions on Power Systems*, vol. 37, pp. 2052-2062, Sept. 2021.

[19] A. Venkatraman, U. Markovic, and D. Shchetinin *et al*., "Improving dynamic performance of low-inertia systems through eigensensitivity optimization," *IEEE Transactions on Power Systems*, vol. 36, pp. 4075-4088, Mar. 2021.

[20] M. H. El-Bahay, M. E. Lotfy, and M. A. El-Hameed, "Effective participation of wind turbines in frequency control of a two-area power system using coot optimization," *Protection and Control of Modern Power Systems*, vol. 8, no. 1, pp. 1-15, Jan. 2023.

[21] S. Gorbachev, J. Guo, and A. Mani *et al*., "MPC-based LFC for interconnected power systems with PVA and ESS under model uncertainty and communication delay," *Protection and Control of Modern Power Systems*, vol. 8, no. 4, pp. 1-17, Oct. 2023.

[22] Z. Wang, W. Wu, and B. Zhang, "A distributed quasi-newton method for droop-free primary frequency control in autonomous microgrids," *IEEE Transactions on Smart Grid*, vol. 9, pp. 2214-2223, Sept. 2016.

[23] H. Mashayekhi, J. Habibi, and T. Khalafbeigi *et al*., "GD cluster: a general decentralized clustering algorithm," *IEEE Transactions on Knowledge and Data Engineering*, vol. 27, pp. 1892-1905, Jul. 2015.

[24] A.B.S. Serapião, G.S. Corrêa, and F.B. Goncalves *et al*. , "Combining K-means and K-harmonic with fish school search algorithm for data clustering task on graphics processing units," *Applied Soft Computing*, vol. 41, pp. 290-304, Apr. 2016.

[25] R. Azimi, H. Sajedi, and M. Ghayekhloo, "A distributed data clustering algorithm in P2P networks," *Applied Soft Computing*, vol. 51, pp. 147-167, Feb. 2017.

[26] Y. Yang, Y. Sun, and Q. Wang *et al*., "Fast power grid partition for voltage control with balanced-depth-based community detection algorithm," *IEEE Transactions on Power Systems*, vol. 37, no. 2, pp. 1612-1622, Mar. 2021.

[27] A. Rosato, R. Altilio and M. Panella, "A decentralized algorithm for distributed ensemble clustering," *Information Sciences*, vol. 578, pp. 417-434, Nov. 2021.

[28] P. Segovia, V. Puig, and E. Duviella *et al*., "Distributed model predictive control using optimality condition decomposition and community detection," *Journal of Process Control*, vol. 99, pp. 54-68, Mar. 2021.

[29] M. E. J. Newman and M. Girvan, "Finding and evaluating community structure in networks," *Physical Review E*, vol. 69, no.2, pp. 2, Feb. 2004.

[30] Z. Chen, Z. Xie, and Q. Zhang, "Community detection based on local topological information and its application in power grid," *Neurocomputing*, vol. 170, pp. 384-392, Dec. 2015.

[31] M. Guerrero, F. G. Montoya, and R. Baños *et al*., "Community detection in national-scale high voltage transmission networks using genetic algorithms," *Advanced Engineering Informatics*, vol. 38, pp. 232-241, Oct. 2018.

[32] Y. Chai, L. Guo, and C. Wang *et al*., "Network partition and voltage coordination control for distribution networks with high penetration of distributed PV units," *IEEE Transactions on Power Systems*, vol. 33, no. 3, pp. 3396-3407, May 2018.

[33] W. Zhang, J. Lian, and C. Chang *et al*., "Aggregated modeling and control of air conditioning loads for demand response," *IEEE Transactions on Power Systems*, vol. 28, no.4, pp. 4655-4664, Jun. 2013.

[34] K. Shimizu, T. Masuta, and Y. Ota *et al*., "Load frequency control in power system using vehicle-to-grid system considering the customer convenience of electric vehicles," in *2010 International Conference on Power System Technology*, Zhejiang, China, Oct. 2010, pp. 1-8.

[35] A. Clauset, M. E. J. Newman, and C. Moore, "Finding community structure in very large networks," *Physical Review E*, vol. 70, no. 6, Dec. 2004.

[36] V. Purba, B. B. Johnson, and S. Jafarpour *et al*., "Dynamic aggregation of grid-tied three-phase inverters," *IEEE Transactions on Power Systems*, vol. 35, no. 2, pp. 1520-1530, Mar. 2019.

[37] Brandes U, Delling D, Gaertler M, *et al*, "On modularity clustering," *IEEE Transactions on Knowledge and Data Engineering*, vol. 20, no. 2, pp. 172-188, Dec. 2007.

[38] Y. Deyou and C. Guowei, "Decentralized model predictive control based load frequency control for high wind power penetrated power systems," *Proceedings of the CSEE*, vol. 35, pp. 583-591, Mar. 2015. (in Chinese)